Available online at www.sciencedirect.com
SCIENCE DIRECT®
Journal of Solid State Chemistry 178 (2005) 2247–2255
JOURNAL OF SOLID STATE CHEMISTRY
www.elsevier.com/locate/jssc

Stabilization of a new δ' polymorph in P-substituted Pb_2BiVO_6: Single crystal structure of $Pb_2Bi(V_{0.84}P_{0.16})O_6$ and conduction properties of related materials

Olfa Labidi, Pascal Roussel*, Marielle Huve, Michel Drache, Pierre Conflant, Jean Pierre Wignacourt

Laboratoire de Cristallochimie et Physicochimie du Solide, UMR CNRS 8012, ENSCL, Université des Sciences et Technologies de Lille—BP 90108, F-59652 Villeneuve d'Ascq Cedex, France

Received 23 February 2005; received in revised form 13 April 2005; accepted 2 May 2005
Available online 6 June 2005

Abstract

The single crystal structure of a new polymorph $\delta' - Pb_2Bi(V_{1-x}P_x)O_6$ has been investigated; on heating, direct phase transitions $\alpha \rightarrow \beta \rightarrow \delta$ and $\alpha \rightarrow \delta$ were identified in $Pb_2Bi(V_{1-x}P_x)O_6$ solid solutions for $x \geqslant 0.10$, thus avoiding the high-temperature form decomposition noted in the ($\delta - Pb_2BiVO_6$) mother phase at 480 °C, to a mixture of $PbBiVO_5$ and Pb_4BiVO_8 before recomposition at 650 °C. Under a slow cooling process, the δ-$Pb_2Bi(V_{1-x}P_x)O_6$ high-temperature phase transforms into a closely related $\delta' - Pb_2Bi(V_{1-x}P_x)O_6$ new polymorph, preserved at room temperature. The structure of $\delta' - Pb_2Bi(V_{0.84}P_{0.16})O_6$ has been solved from a single crystal data in the orthorhombic system, *Pbca* space group, with $a = 5.922(1)$ Å, $b = 18.395(5)$ Å, $c = 11.864(3)$ Å, $Z = 8$, and compared to a previous description of $\delta - Pb_2BiVO_6$ in *Pmcn*, with b lattice constant halved. Complementary structural investigations of $\delta' - Pb_2Bi(V_{0.75}P_{0.25})O_6$ powder sample by the Rietveld method, and TEM diffraction studies, confirmed the lattice and space group settings. The structural relationship between the α, δ and δ' forms is completed for $Pb_2Bi(V_{1-x}P_x)O_6$, and ionic conductivity versus temperature has been measured in the new phase as well as in its related solid solutions.

Keywords: Pb2BiVO$_6$; Solid solution; Phase stabilization; Single crystal structure; Oxide ionic conduction

1. Introduction

Pb_2BiVO_6 exhibits several polymorphic forms labeled α to δ [1]. The α phase was obtained after air quenching of a stoiechiometric reaction product from 700 °C. The thermal evolution of α studied by differential thermal analysis (DTA) and high-temperature X-ray diffraction (HTXRD) shows three modifications, $\alpha \rightarrow \beta \rightarrow \gamma \rightarrow \delta$. The γ variety was shown to be a mixture of Pb_4BiVO_8 and of the high-temperature monoclinic form of $PbBiVO_5$ [2].

Recently, the crystal structures of the room temperature α form, and of the high temperature δ form at 680 °C were solved from powder diffraction data by simulated annealing methods applied to combined X-ray and high-resolution powder neutron diffraction data [3,4]. The phase transitions $\alpha \rightarrow \beta$ and $\beta \rightarrow \delta$ were identified in the mother phase Pb_2BiVO_6 as well as in $Pb_2BiV_{1-x}M_xO_{6\pm y}$ solid solutions (M = Cr, Mn) [5]; the high-temperature form $\delta - Pb_2BiVO_6$ eventually decomposes at 480 °C to a mixture of $PbBiVO_5$ and Pb_4BiVO_8 before showing recombination at 650 °C in δ form.

In this paper, new features are described about: the stabilization of an original variety δ' of the high-temperature form obtained through the partial substitution of P for V in Pb_2BiVO_6; the crystal structure determination from X-ray diffraction data of a single crystal for the new $\delta' - Pb_2Bi(V_{0.84}P_{0.16})O_6$ phase stabilized at room temperature, and finally the conduction

*Corresponding author.
E-mail address: pascal.roussel@ensc-lille.fr (P. Roussel).

0022-4596/$ - see front matter © 2005 Elsevier Inc. All rights reserved.
doi:10.1016/j.jssc.2005.05.003

properties of $Pb_2Bi(V_{1-x}M_x)O_{6\pm y}$ (M = P, Cr, Mn) and $Pb_{1.9}Mn_{0.1}BiVO_{6\pm y}$ related compounds compared to Pb_2BiVO_6.

2. Experimental

2.1. Synthesis

Samples of $(Pb_{2-x}Mn_x)BiVO_{6\pm y}$ were prepared from stoiechiometric proportions of PbO (Riedel de Haën, 99%), Bi_2O_3 (Aldrich, 99.9%), V_2O_5 (Aldrich, 99.6%), and MnO_2 (Aldrich, 99%), sealed in an evacuated silica ampoule and heated at 700 °C for 30 h. $Pb_2Bi(V_{1-x}P_x)O_6$, compositions were synthesized with $(NH_4)_2HPO_4$ (Sigma, 99%) and were preheated at 280 °C, then at 570 °C with intermediate grindings; the M = Cr, Mn, related compounds were obtained as described previously [5]. Finally in both cases, the specimens were held at 700 °C for 4 days and then air quenched. The completeness of the reaction was checked by X-ray diffraction (XRD). Single crystals were grown out of sample powders of nominal compositions of $Pb_2BiV_{0.85}P_{0.15}O_6$. The powders were placed in gold tubes and maintained at 850 °C for 12 h, cooled at 2 °C/h to 750 °C, then at 5 °C/h to room temperature.

2.2. Characterization

Density measurements were performed with an automated Micrometrics Accupyc 1330 helium pycnometer in a 1 cm^3 cell. The HTXRD diagrams were measured using a Guinier–Lenné diffraction system with Cu$K\alpha$1 radiation to determine whether any phase transitions exist. The X-ray diffraction patterns were collected using a Siemens D5000 powder diffractometer using a Bragg–Brentano geometry, with a diffracted beam monochromator and Cu$K\alpha$ radiation. An attachment of an Anton Paar HTK 1200 high-temperature oven and a scintillation detector enabled data acquisition from room temperature to 700 °C. Differential thermal analysis was performed with a TG/DT 92 SETARAM instrument. Electron Micro Probe Analysis (EMPA) of the single crystal used for XRD data collection was made on a microprobe Camebax-Microbeam device (1SI-2S2) from Cameca-France, working in Wavelength Dispersive Spectrometry mode; the analyzers crystals used were, respectively: pentaerythrite (PET) for Mα of Pb and Bi, thallium biphtalate (TAP) for $K\alpha$ of P, (lithium fluoride) LiF for $K\alpha$ of V, and the weight concentrations of the elements were calibrated respectively from Bi_2O_3, $Ca_5F(PO_4)_3$ and $Pb_5(VO_4)_3Cl$. Selected area electron DIFFRACTION (SAED) patterns were obtained on a JEOL 200CX transmission electron microscope. The materials were crushed and dispersed on a holey carbon film deposited on a Cu grid.

For conductivity measurements, powder samples were pelletized at room temperature and then sintered 50 °C below their melting point for 48 h. Gold electrodes were sputtered on both flat faces and measurements were done by impedance spectrometry in the frequency range 1–10^6 Hz with a Schlumberger 1170 frequency response analyzer.

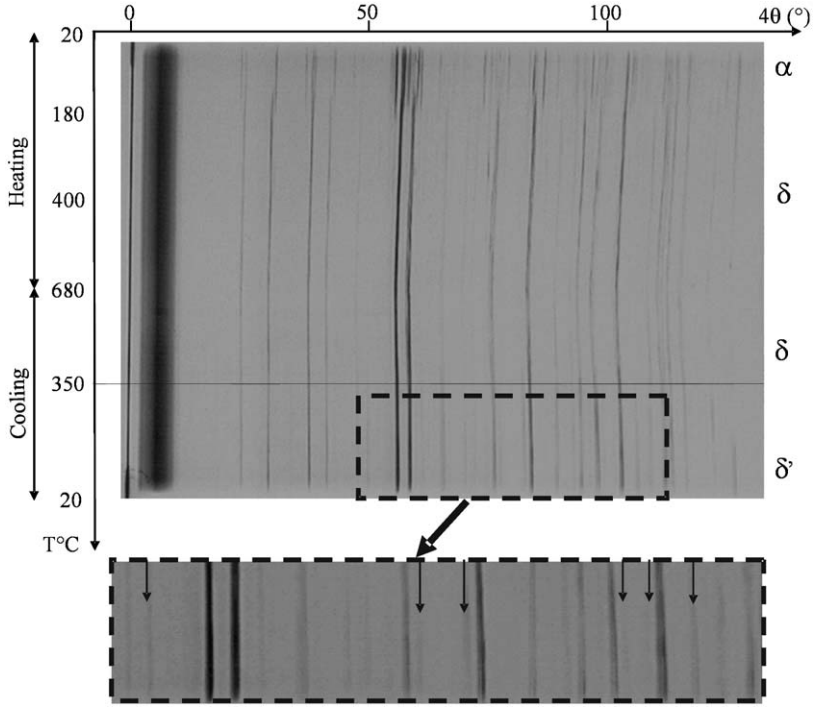

Fig. 1. Guinier Lenné film showing the simplified phase transition sequence in $Pb_2Bi(V_{0.85}P_{0.15})O_6$. Inset of the $\delta \rightarrow \delta'$ is highlighted.

The behavior of the new δ' phase was investigated by dilatometry analysis (Linseis L75 dilatometer) with a heating rate of 5 °C/min to 700 °C and 5 °C/min cooling rate in air.

3. Results

3.1. Solid solution domains, high temperature form stabilization and thermal behavior

Several substitutions have been tested in order to investigate the stabilization of the high temperature form at lower temperatures.

3.1.1. $(Pb_{2-x}Mn_x)BiVO_{6\pm y}$ samples

Powder samples of $(Pb_{2-x}Mn_x)BiVO_{6\pm y}$ compositions were prepared for $0 \leqslant x \leqslant 1$. A single-phase material was obtained up to the limit of substitution at $x = 0.10$. In this solid solution domain, the transition sequence $\alpha \rightarrow \beta \rightarrow \delta \rightarrow \gamma \rightarrow \delta$ is equivalent to that of unsubstituted Pb_2BiVO_6, i.e. showing the γ intermediate decomposition into related $PbBiVO_5$ and Pb_4BiVO_8 type phases. In the interval $0.1 < x \leqslant 1$ at room temperature, some extra peaks belonging to two other phases: $BiPbVO_5$ and Mn_3O_4, appeared systematically in the powder patterns.

3.1.2. $Pb_2Bi(V_{1-x}P_x)O_6$ samples

Previous investigations have shown that P and As can be substituted isomorphously for V [6,7]. Therefore $Pb_2Bi(V_{1-x}P_x)O_6$ compositions were synthesized over the full range $0 \leqslant x \leqslant 1$. Steps of 0.02 were used in the interval $0 \leqslant x \leqslant 0.2$.

At room temperature powder patterns of all the samples are similar to the pattern of $\alpha - Pb_2BiVO_6$ in the interval $0 \leqslant x \leqslant 0.15$. A mixture of α and δ'-type phases was observed for $x = 0.16$ and 0.18.

For $x = 0.06$, the thermal evolution is similar to that of the unsubstituted phase. Starting at $x = 0.10$ (i.e. $Pb_2Bi(V_{0.90}P_{0.10})O_6$), the transition sequence simplifies to $\alpha \rightarrow \beta \rightarrow \delta$. The δ form is observed below 500 °C and transforms into the room temperature α form by air quenching. For the composition $x = 0.15$, the sequence is further simplified on heating by the direct transition $\alpha \rightarrow \delta$, which is observed at 180 °C (Fig. 1). Under slow cooling conditions ($\approx$ 15 °C/h) the δ form transforms into a closely related δ' form, which is preserved at room temperature and thus can be characterized.

3.2. Structural analyses

3.2.1. X-ray single crystal data

A well-shaped yellow single crystal ($0.06 \times 0.03 \times 0.015$ mm) was selected for the crystal structure investigation out of a preparation from the initial nominal composition $Pb_2BiV_{0.85}P_{0.15}O_6$. Single crystal X-ray diffraction intensities were measured out of this yellow crystal on a Bruker SMART CCD detector diffractometer, Mo $K\alpha$ radiation, under the conditions shown in Table 1. The reported lattice parameters were refined from the complete single crystal data set. All of them are closely related to the cell parameters of the

Table 1
Crystal data and structure refinement for δ'-$Pb_2Bi(V_{0.84}P_{0.16})O_6$

Formula	$Pb_2Bi(V_{0.84}P_{0.16})O_6$
Formula weight ($g\,mol^{-1}$)	767.10
Crystal system	Orthorhombic
Space group	*Pbca* (No. 61)
Unit cell dimensions (Å)	$a = 5.922(1)$
	$b = 18.395(5)$
	$c = 11.864(3)$
Cell volume ($Å^3$)	1292(1)
Z	8
Density calculated/measured ($g\,cm^{-3}$)	7.88/7.85(3)
F000	2533
Intensity collection	
Wave length (Å)	0.71073 (Mo $K\alpha$)
θ range (deg)	4–29.83
Data collected	$-8 \leqslant h \leqslant 8$; $-16 \leqslant k \leqslant 16$; $-25 \leqslant l \leqslant 24$
No. of reflections measured	8067
No. of independent ($I > 3\sigma(I)$)	1723
μ_1 (Mo $K\alpha$) mm^{-1}	82.14
T_{max}/T_{min} ratio	0.119
R_{int} (obs/all) before absorption correction	0.2636/0.2706
R_{int} (obs/all) after absorption correction	0.1062/0.1195
Refinement	
No. of parameters	62
Weighting scheme	$1/\sigma^2$
Goodness of fit obs/all	1.34/1.92
$R(F)$ obs/all	0.0509/0.1438
$wR(F)$ obs/all	0.0428/0.0495
ρ_{max}, ρ_{min} (e^-/Å)	4.57, −5.52
Extinction coefficient	0.024(1)

Table 2
Atomic coordinates and isotropic/equivalent displacements parameters ($Å^2$) for δ'-$Pb_2Bi(V_{0.84}P_{0.16})O_6$

Atom	x	y	z	U_{iso}/U^*_{eq}
Pb1	0.7620(2)	0.28200(5)	0.3532(1)	0.0248(3)*
Bi2	0.2430(2)	0.13594(5)	0.3488(1)	0.0227(3)*
Pb3	0.2048(2)	0.98726(5)	0.1464(1)	0.0300(4)*
(V,P)	0.7641(8)	0.1227(3)	0.5610(5)	0.031(2)*
O1	0.442(3)	0.0603(8)	0.240(2)	0.024(4)
O2	0.668(4)	0.126(1)	0.692(2)	0.074(8)
O3	0.009(3)	0.2097(8)	0.242(2)	0.025(4)
O4	0.588(4)	0.083(1)	0.480(3)	0.074(8)
O5	0.837(5)	0.203(1)	0.513(3)	0.11(1)
O6	0.987(6)	0.073(2)	0.546(4)	0.15(2)

Table 3
Atomic displacement parameters (Å^2) for δ'-$Pb_2Bi(V_{0.84}P_{0.16})O_6$

Atom	U_{11}	U_{22}	U_{33}	U_{12}	U_{13}	U_{23}
Pb1	0.0226(5)	0.0215(5)	0.0304(7)	0.0030(4)	−0.0005(8)	−0.0048(6)
Bi2	0.0201(5)	0.0261(5)	0.0217(6)	0.0036(4)	0.0016(8)	0.0004(6)
Pb3	0.0242(5)	0.0230(5)	0.0427(9)	−0.0013(4)	−0.0057(7)	−0.0098(7)
(V,P)	0.025(2)	0.037(3)	0.030(3)	−0.011(3)	−0.004(3)	−0.001(3)

Table 4
Selected bond distances (Å) for δ'-$Pb_2Bi(V_{0.84}P_{0.16})O_6$

Pb1—O2^{i}	2.99(2)	Pb3—O6^{xii}	2.45(4)
Pb1—O2^{ii}	2.61(2)	(V,P)—O2	1.66(2)
Pb1—O3^{iii}	2.38(2)	(V,P)—O4	1.60(3)
Pb1—O3^{iv}	2.30(2)	(V,P)—O5	1.64(2)
Pb1—O5	2.43(3)	(V,P)—O6	1.62(4)
Pb1—O5^{v}	2.99(3)	O1—O1^{vi}	2.97(3)
Bi2—O1	2.23(2)	O1—O1^{iv}	2.97(3)
Bi2—O1^{vi}	2.49(2)	O1—O3^{iv}	2.79(2)
Bi2—O3	2.32(2)	O2—O4	2.68(4)
Bi2—O3^{iv}	2.34(2)	O2—O5	2.74(4)
Bi2—O4	2.75(3)	O2—O6	2.74(5)
Bi2—O6^{vii}	3.02(4)	O3—O3^{vi}	2.97(3)
Pb3—O1^{viii}	2.24(2)	O3—O3^{iv}	2.97(3)
Pb3—O1^{ix}	2.46(2)	O4—O5	2.68(3)
Pb3—O2^{x}	2.93(2)	O4—O6	2.50(4)
Pb3—O4^{ix}	2.41(3)	O5—O6	2.58(4)
Pb3—O4^{xi}	2.93(3)	O6—O6^{xiii}	2.90(5)

Symmetry transformations used to generate equivalent atoms: (i) $0.5+x$, $0.5-y$, $1-z$; (ii) x, $0.5-y$, $-0.5+z$; (iii) $1+x$, y, z; (iv) $0.5+x$, y, $0.5-z$; (v) $-0.5+x$, $0.5-y$, $1-z$; (vi) $-0.5+x$, y, $0.5-z$; (vii) $-1+x$, y, z; (viii) x, $1+y$, z; (ix) $-0.5+x$, $1+y$, $0.5-z$; (x) $1-x$, $1-y$, $1-z$; (xi) $0.5-x$, $1-y$, $-0.5+z$; (xii) $1.5-x$, $1-y$, $-0.5+z$; (xiii) $2-x$, $-y$, $1-z$.

$\delta - Pb_2BiVO_6$ phase given by Evans et al. [4], but the b parameter doubled. Elemental analyses (EMPA) performed on this specific crystal over 20 points have shown that the distribution is homogenous, with mean atomic ratio that are, respectively $Pb/Bi \cong 2$, $Bi/(V+P) \cong 1$ and $V/P = 5.2$; therefore it was identified as $Pb_2Bi(V_{0.84}P_{0.16})O_6$. Therefore we labeled this new compound $\delta' - Pb_2Bi(V_{0.84}P_{0.16})O_6$. An absorption correction based on the redundancy algorithm [8], was applied to the set of raw intensities using the program SADABS (Siemens Area Detector ABSorption correction [9]) leading to a decrease of the internal consistency factor $R(F^2)_{int}$, respectively from 26.36% to 10.62% for the studied crystal. The pertinent data are summarized in Table 1.

The structure was solved by direct methods using the SIR97 software [10], which readily established the heavy atom positions (Pb, Bi, V). The V/P ratio identified by EMPA was introduced as a mixed occupancy of the corresponding site, and not refined. Oxygen atoms were localized from different Fourier maps. The last cycles of refinement included atomic positions, anisotropic displacement parameters for all non-oxygen atoms, and isotropic displacement parameters for oxygen atoms. Full-matrix least-squares structure refinements against F were carried out using the JANA 2000 [11] program. The results of the refinement are presented in Tables 2–3 and the main bond distances are listed in Table 4.

3.2.2. *Crystal structure of* $\delta' - Pb_2Bi(V_{0.84}P_{0.16})O_6$

The crystal structure obtained for $\delta' - Pb_2Bi(V_{0.84}P_{0.16})O_6$ is shown in Fig. 2. It could be described with the formalism used for the related M_2BiPO_6 oxyphosphates compounds [12] in terms of D/D sequence, that is a succession (along b) of double infinite ribbons (along a) built on edged-shared $O(Bi,Pb)_4$ tetrahedra and surrounded by six phospho-vanadate groups.

However, a more detailed description can be done: the Bi coordination may be visualized as a triangular prism with one base formed by $2 \times O1$ and $2 \times O3$ oxygen atoms at distances ranging from 2.23(2) to 2.49(2) Å; two other atoms (O4 as a corner shared with one (V,P)O4 tetrahedron, and O6 as a second one from a different $(V,P)O_4$) are located on the opposite side, respectively at distances 2.75(3), 3.02(4) Å, leaving available space for the lone pair location. The coordination around Pb1 describes a distorted 6-fold (pseudo-octahedral) coordination, with O3–O3 as one edge, and twice O2 and O5 as four corners shared with 4 different $(V,P)O_4$. A 7-fold coordination is observed around Pb3 with O1–O1 as an edge completed by O2–O4 as the edge of one phospho-vanadate group, O6 as the apex of a second one, and by O4 and O2 as two single links to a third and a fourth $(V,P)O_4$.

As previously described in the related room temperature form $\alpha - Pb_2BiVO_6$ (from either powder data [4] or single crystal [5]) the common feature is the existence of infinite ribbons ($O_2Bi_2Pb_4$) built of O1(2Bi 2Pb3) and O3(2Bi 2Pb1) edge-sharing cationic tetrahedral units. Independent $(V,P)O_4$ tetrahedra are bridging these ribbons as described in the heavy atoms coordination polyhedra; each terminal lead Pb1 and Pb3 is involved, respectively, with four and three neighboring $(V,P)O_4$: Pb1 through one apex each, and Pb3, respectively, through one edge, and twice through one apex. The central Bi2 is capped by two phospho-vanadate units through one apex each.

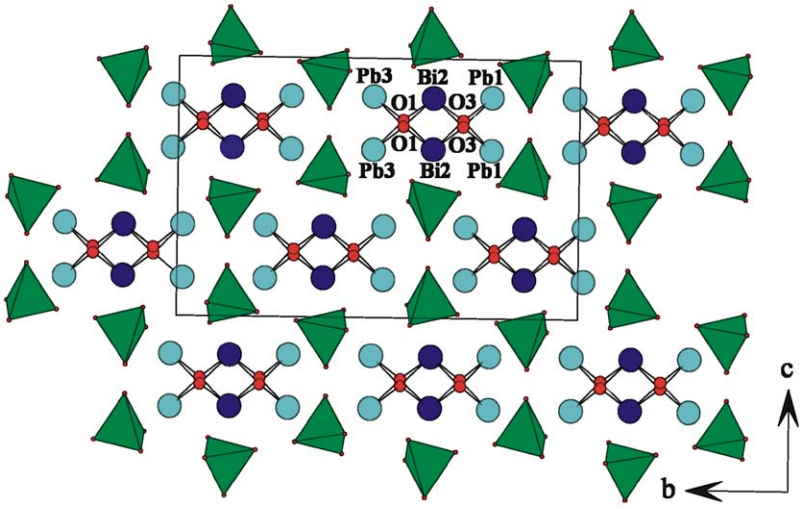

Fig. 2. Projection along [100] of the structure $\delta' - Pb_2Bi(V_{0.84}P_{0.16})O_6$.

Table 5
Lone pairs localization in δ'-$Pb_2Bi(V_{0.84}P_{0.16})O_6$

	x	y	z	d_{core}–L(Å)
Pb1	0.763	0.314	0.375	0.650
Bi2	0.191	0.132	0.406	0.746
Pb3	0.229	0.963	0.111	0.624

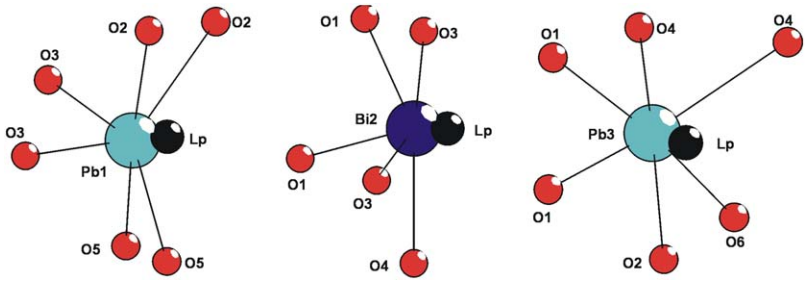

Fig. 3. View of cationic oxygen coordination polyhedra in $\delta' - Pb_2Bi(V_{0.84}P_{0.16})O_6$, including the Bi/Pb lone pair positions.

The location of the lone pair (Lp) of bismuth and lead atoms has been calculated with the program HYBRIDE developed by Morin et al. [13]. Verbaere et al. [14] proposed a method to determine the displacement of the ns^2 lone pair from cation cores leading to the basic formula of the induced polarization P, $P = -2d = \alpha E$, where -2 is the charge of the lone pair, d the core-lone pair distance, α the polarizability of the considered atom, and E the local electrostatic field calculated by Ewald's method [15]. According to Shannon [16], the polarizability of lead and bismuth are, respectively, 6.58 and 6.12 $Å^3$. The Pauling formula [17] has allowed to calculate the ionicity ratio of each bond, from the electronegativity difference taken from Allred and Rochow [18], giving charges of $+1.23$, $+1.73$, $+3.25$, $+2.05$ for Pb, Bi, V, P atoms, respectively. The different oxygen atoms were given the balancing -1.21 charge providing electroneutrality. Calculations reached self-consistent positions for the three atoms listed in Table 5, Fig. 3.

3.2.3. Comparison of α, δ and δ′ polymorphs

A comparison has been made between the room temperature description of $\delta' - Pb_2Bi(V_{0.84}P_{0.16})O_6$ in *Pbca* (this work), and the high-temperature $\delta - Pb_2BiVO_6$ [4] in *Pmcn*, at 680 °C. The literature model was introduced in the refinement of our single crystal data set, with our b lattice constant halved: the oxygen

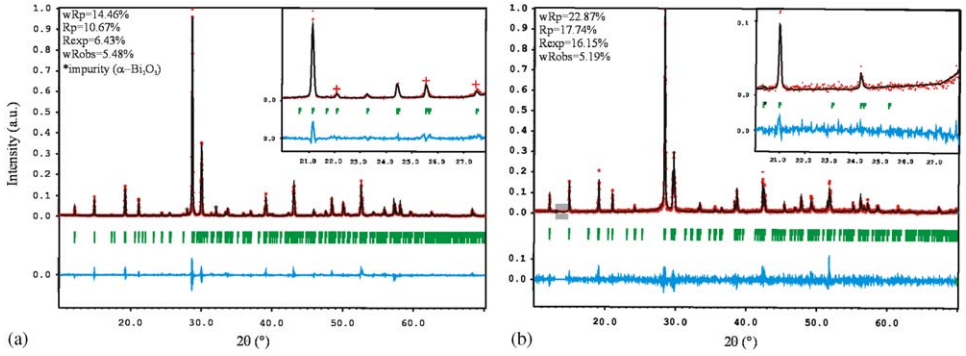

Fig. 4. Observed and calculated X-ray diffraction pattern after the Rietveld treatment for room temperature δ'-$Pb_2BiV_{0.75}P_{0.25}O_6$ (a), and δ-$Pb_2BiV_{0.75}P_{0.25}O_6$ at 700 °C (b). In the inset are shown the "extra" peaks observed in δ' compared to δ.

position parameters did not refine and the R factor increases to 0.13. In a *Pmca* trial, the global R factor decreases to 0.10, but the $(V,P)O_4$ oxygen positions did not refine either. Then a structure refinement by the Rietveld method was carried out on X-ray diffraction powder data of a $Pb_2BiV_{0.75}P_{0.25}O_6$ sample. At room temperature, the results confirmed our δ' crystal setting; when based on the δ-type mean unit cell, either in the *Pmcn* or *Pmca* space groups, some weak intensity peaks are not included in the refinement process (see inset of Fig. 4). The obtained agreement factors under the *Pbca* setting were: overall $wR_p = 14.46\%$, $R_p = 10.67\%$, $R_{exp} = 6.43\%$, and $wR_{obs} = 5.48\%$. At high temperature, the results were coherent with the $\delta - Pb_2BiVO_6$-type literature model in *Pmcn*. The final Rietveld plots of the two polymorphs are compared for $\delta' - Pb_2Bi(V_{0.75}P_{0.25})O_6$ Fig. 4(a) and $\delta - Pb_2Bi(V_{0.75}P_{0.25})O_6$ Fig. 4(b).

Moreover, an electron diffraction study confirms the δ' setting: it allows the unambiguous determination of the lattice parameters as well as the evidence of an helicoïdal axis, and by comparison of the zero order Laue zone (ZOLZ) and first-order Laue zone (FOLZ) the Bravais lattice and the existence of glide planes [19]. The comparison (Fig. 5) between the periodicity and the shifting of the ZOLZ and the FOLZ leads to the extinction symbol *Pbca*, which is in accordance with the space group used for the structural refinement. For all the basic zone axes, i.e. [100], [010], and [001] no shift but a difference of periodicity schematically represented with a white rectangle in Fig. 5 is noted, indicating a P Bravais lattice and the presence of three glide planes.

These results made possible the comparison of the structures of $\alpha - Pb_2BiVO_6$ and $\delta' - Pb_2Bi(V_{0.84}P_{0.16})O_6$ at room temperature in order to identify their linkage through the $\alpha \rightarrow \delta$ and $\delta \rightarrow \delta'$ phase transition process. While their preserved common structural characteristic is the infinite ribbon of $O_2Bi_2Pb_4$, there are, respectively, 4 crystallographically independent tetrahedral oxygens in the α form and 2 in the δ' form stabilized at room temperature, while only one appears at high temperature

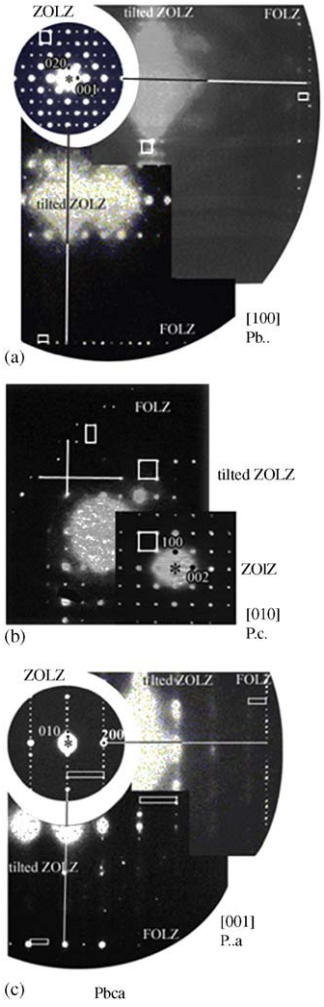

Fig. 5. (a) [100], (b) [010], (c) [001] zone axis patterns. The comparison of the shift and difference of periodicity between the zero-order Laue zone (ZOLZ) and the first-order Laue zone (FOLZ) leads to the *Pbca* extinction symbol. Due to the relatively large reciprocal parameters of the compounds a tilting of the ZOLZ is necessary to observe the FOLZ on the same pattern.

in the δ form. These ribbons are surrounded by 6 VO_4 tetrahedra with different orientations, going from 2 different crystallographically unique VO_4 [4] in the α

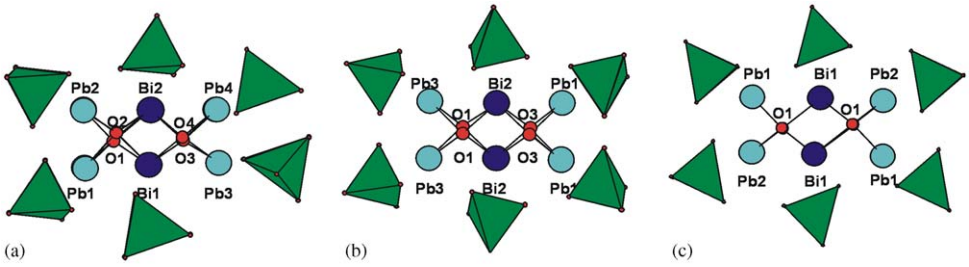

Fig. 6. Comparison of the $(O_2Bi_2Pb_2)_\infty$ ribbons and their VO_4 surrounding in $\alpha - Pb_2BiVO_6$ (a), $\delta' - Pb_2Bi(V_{0.84}P_{0.16})O_6$ (b) and $\delta - Pb_2BiVO_6$ (c).

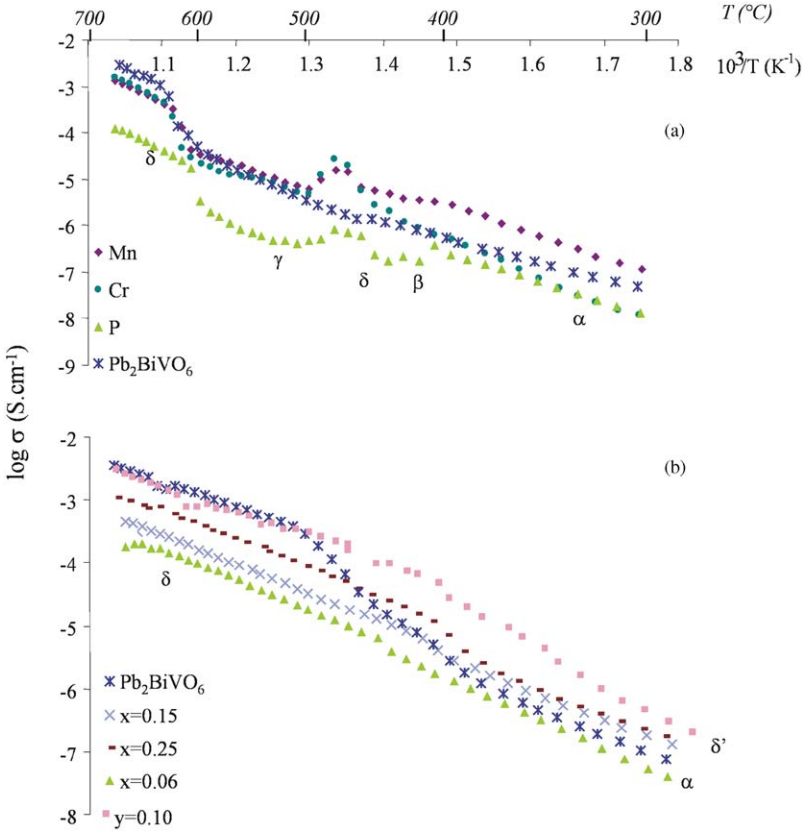

Fig. 7. First heating (a) and first cooling (b) Arrhenius plots for $Pb_2BiV_{1-x}M_{0.06}O_{6\pm y}$ (a), $Pb_2BiV_{1-x}P_xO_6$ (b) and $Pb_{1-y}Mn_yBiVO_{6\pm y}$ (b).

form, to only one unique $(V,P)O_4$ in δ' or VO_4 in the δ form. In the crystal structure of α-$Pb_2Bi(V_{0.94}Mn_{0.06})O_{6\pm y}$ [5] the two unique $(V,Mn)O_4$ clusters are showing two statistically disordered orientations each, while in this study the $(V,P)O_4$ is ordered. The second main difference between the structures of these three Pb_2BiVO_6-related polymorphs arises from the orientations of the isolated VO_4 or phospho-vanadate tetrahedral groups, Fig. 6.

3.3. Conduction properties

Conductivity measurements were done on Pb_2BiVO_6 and substituted compounds; the resulting Arrhenius plots corresponding to typical examples are shown in Fig. 7. The electrical characteristics (conductivity and activation energies) determined for low- and high-temperature forms, are summarized in Table 6; these data could not be evaluated for the intermediate phases, due to the narrowness of the corresponding domains. For Pb_2BiVO_6, as well as for $Pb_2BiV_{0.94}M_{0.06}O_{6\pm y}$ (M = P, Mn, Cr) samples (Fig. 7a), the transition sequence $\alpha \rightarrow \beta \rightarrow \delta \rightarrow$ decomposition $\rightarrow \delta$ is observed during the first heating run. For the considered substitution rate, i.e. $x = 0.06$, the Cr-doped high-temperature form exhibits the best conductivity level.

In the case of P substituting for V, the increase of the substitution rate allows the direct $\alpha \rightarrow \delta$ transition

Table 6
Activation energies and conductivities on heating* and on cooling at 300 °C (α or δ') and 690 °C (δ)

	300 °C		690 °C	
	E_a (eV)	σ (S cm^{-1})	E_a (eV)	σ (S cm^{-1})
Pb_2BiVO_6	0.81*	$4{,}80 \times 10^{-8}$*	1,42*	$3{,}41 \times 10^{-3}$
	0.89	$7{,}63 \times 10^{-8}$	0,83	
$Pb_2BiV_{0.94}Cr_{0.06}O_{6\pm y}$*	1.07	$1{,}18 \times 10^{-8}$	1,17	$1{,}60 \times 10^{-3}$
$Pb_2BiV_{0.94}Mn_{0.06}O_{6\pm y}$*	1.09	$1{,}15 \times 10^{-7}$	1,55	$1{,}30 \times 10^{-3}$
$Pb_2BiV_{0.94}P_{0.06}O_6$	1.48*	$3{,}83 \times 10^{-8}$*	1,59*	$1{,}19 \times 10^{-4}$
	1.23	$1{,}31 \times 10^{-8}$	0,98	
$Pb_2BiV_{0.85}P_{0.15}O_6$	0.92	$1{,}34 \times 10^{-7}$	0,97	$4{,}43 \times 10^{-4}$
$Pb_2BiV_{0.75}P_{0.25}O_6$	0.92	$1{,}69 \times 10^{-7}$	1	$1{,}05 \times 10^{-3}$
$Pb_{1.9}Mn_{0.1}BiVO_{6\pm y}$	1.25	$1{,}98 \times 10^{-7}$	0,84	$3{,}01 \times 10^{-3}$

($x = 0.15$), and avoids the intermediate decomposition of the high-temperature phase during the heating run. Two steps have to be considered for the high-temperature range: a first one in the vanadium rich region (at least $0 \leqslant x \leqslant 0.06$) which occurs with a decrease of conductivity for the δ phase, and a second one ($0.15 \leqslant x \leqslant 0.25$) leading to an increase of σ; which nevertheless does not reproduce the $\delta - Pb_2BiVO_6$ initial performances. The Arrhenius plots corresponding to the first cooling run are presented for $Pb_2BiV_{1-x}P_xO_6$ ($x = 0$; 0.15; 0.25) samples (Fig. 7b). For $x = 0.15$, 0.25, two pseudo-linear domains with a $\delta \rightarrow \delta'$ transition zone are observed nearby 425 °C. This behavior can be associated with the $\delta \rightarrow \delta'$ modification observed around 350 °C in the cooling part of the $Pb_2BiV_{0.85}P_{0.15}O_6$ Guinier Lenné pattern (Fig. 1); a subsequent reheating of the same sample shows again the $\delta' \rightarrow \delta$ transformation. The existence of this structural modification is also noted on the dilatometry curve of a pelletized sample of $Pb_2BiV_{0.75}P_{0.25}O_6$, Fig. 8.

In the case of Mn for Pb substitution, the presented Arrhenius plot corresponds to the first cooling run of a $Pb_{1.9}Mn_{0.1}BiVO_{6\pm y}$ sample (Fig. 7b). Two nearly linear domains are observed and can be distinguished by a change in the activation energy at about 420 °C. The X-ray diffraction pattern of the pellet, powdered at the end of the conductivity measurements, is characteristic of the δ'-phase.

It is worthwhile to note the improvement of the final conductivity ($\cong$ half a decade) observed for various substituted samples compared to Pb_2BiVO_6 which results from the stabilization of the high conducting δ'-type phase altogether with the disappearance of the $\delta \rightarrow \alpha$ transformation. In the low temperature range, the Mn for Pb substitution induces the best σ improvement. Complementary investigations are under progress in order to identify the conduction mechanism, either of purely ionic or mixed ionic/electronic nature.

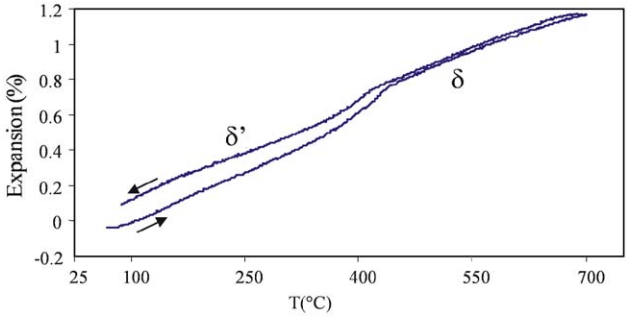

Fig. 8. Dilatometry curve of $Pb_2BiV_{0.75}P_{0.25}O_6$ showing the $\delta' \Leftrightarrow \delta$ transition.

Acknowledgments

We are indebted to Dr. Olivier Mentré (LCPS) for fruitful discussions on this research topic, and to Dr. Didier Le Maguer for the EMPA investigations. The authors would like to thank the referees for constructive remarks.

The crystallographic data have been deposited and can be obtained through the FIZ data bank, on quoting the depository number: CSD415044.

References

[1] A. Mizrahi, J.P. Wignacourt, M. Drache, P. Conflant, J. Mater. Chem. 5 (6) (1995) 901.
[2] S. Giraud, A. Mizrahi, M. Drache, P. Conflant, J.P. Wignacourt, H. Steinfink, Solid State Sci. 3 (2001) 593.
[3] I. Radosavljevic Evans, J.A.K. Howard, R.L. Withers, J.S.O. Evans, Chem. Comm. 19 (2001) 1984.
[4] I. Radosavljevic Evans, J.S.O. Evans, J.A.K. Howard, J. Mater. Chem. 12 (2002) 2648.
[5] O. Labidi, J.P. Wignacourt, P. Roussel, M. Drache, P. Conflant, H. Steinfink, Solid State Sci. 6 (2004) 783–790.
[6] P. Roussel, S. Giraud, E. Suard, J.P. Wignacourt, H. Steinfink, Solid State Sci. 4 (2002) 1143.

[7] S. Giraud, S. Obbade, E. Suard, H. Steinfink, J.P. Wignacourt, Solid State Sci. 5 (2003) 335.
[8] R.H. Blessing, Acta Cryst. A 51 (1995) 33.
[9] G. Sheldrick, SADABS 2.03, University of Göttingen, Germany, 2002.
[10] A. Altomare, G. Cascaro, C. Giacovazzo, A. Guagliardi, M.C. Burla, G. Polidori, M. Camalli, "SIR97", J. Appl. Crystallogr. 27 (1994) 434.
[11] V. Petricek, M. Dusek, JANA2000. Institute of Physics, Praha, Czech Republic, 2002.
[12] F. Abraham, O. Cousin, O. Mentre, El.M. Ketatni, J. Solid State Chem. 167 (2002) 168.
[13] E. Morin, G. Wallez, S. Jaulmes, J.C. Couturier, M. Quarton, J. Solid State Chem. 137 (1998) 283.
[14] A. Verbaere, R. Marchand, M. Tournoux, J. Solid State Chem. 23 (1978) 383.
[15] P.P. Ewald, Ann. Phys. 64 (1921) 253.
[16] R.D. Shannon, J. Appl. Phys. 73 (1993) 348.
[17] L. Pauling, The Nature of the Chemical Bond, Cornell University Press, New York, 1939.
[18] A.L. Allred, E.G. Rochow, J. Inorg. Nucl. Chem. 5 (1958) 264.
[19] J.P. Morniroli, J.W. Steeds, Ultramicroscopy 45 (1992) 219.